Journal of Colloid and Interface Science 538 (2019) 349–356

Contents lists available at ScienceDirect

Journal of Colloid and Interface Science

journal homepage: www.elsevier.com/locate/jcis

Regular Article

One-pot synthesis of highly branched Pt@Ag core-shell nanoparticles as a recyclable catalyst with dramatically boosting the catalytic performance for 4-nitrophenol reduction

Zhi-Suo Lv, Xiao-Yan Zhu, Han-Bin Meng, Jiu-Ju Feng, Ai-Jun Wang *

Key Laboratory of the Ministry of Education for Advanced Catalysis Materials, College of Chemistry and Life Sciences, College of Geography and Environmental Sciences, Zhejiang Normal University, Jinhua 321004, China

GRAPHICAL ABSTRACT

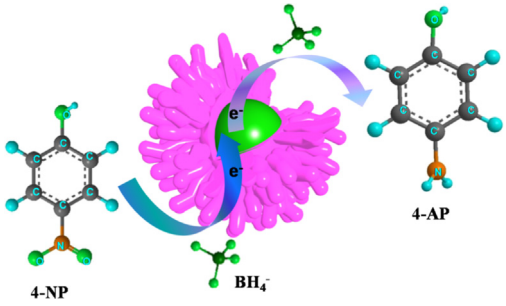

ARTICLE INFO

Article history:
Received 31 August 2018
Revised 29 November 2018
Accepted 30 November 2018
Available online 1 December 2018

Keywords:
Wet-chemical approach
Core-shell nanoparticles
4-Nitrophenol
Catalysis

ABSTRACT

Herein, highly branched Pt@Ag core-shell nanoparticles (Pt@Ag NPs) were fabricated by a facile one-pot wet-chemical approach, where poly(ethyleneimine) (PEI) served as structure-directing and capping agents. Their structure, morphology and composition were mainly characterized by a set of techniques. And their growth mechanism was discussed in some detail. The prepared catalyst exhibited remarkable enhancement in catalytic activity of 4-nitrophenol (4-NP) reduction as a proof-of-concept application, surpassing commercial Pt black and home-made Ag NPs catalysts. Also, the as-obtained catalyst showed superior stability without sacrificing the catalytic activity. These observations endow the catalyst possibility for practical applications in nitrophenols environmental remediation.

1. Introduction

As one of the most refractory pollutants, nitrophenols are widely existed in environment, which can severely damage human health, and endanger central nervous system, liver, kidney and blood [1]. Most notably, 4-nitrophenol (4-NP) and its derivatives are formed from the production processes of pesticides, herbicides and synthetic dyes [2]. Hence, various methods have been developed for transferring 4-NP to harmless products such as 4-aminophenol (4-AP, which usually works as photographic developer, anticorrosion lubricant and intermediate for medicine), including photodegradation [3], chemical reduction [4], biodegradation [5], and solid-phase extraction [6]. Among these methods, extensive attention was paid on catalyzing the hydrogenation of 4-NP to directly produce 4-AP by the aid of sodium borohydride ($NaBH_4$) [7]. Therefore, mild and economical catalysts are essential to enhance the conversion efficiency in these researches.

Recently, noble metals (e.g. Au, Ag, and Pd) have gained substantial attention for 4-NP reduction [8]. For instance, Zhao et al.

* Corresponding author.
E-mail address: ajwang@zjnu.cn (A.-J. Wang).

https://doi.org/10.1016/j.jcis.2018.11.109
0021-9797/

prepared Ag NPs on halloysite nanotubes for catalytic reduction of 4-NP [9]. Naik and his coworkers synthesized Ag NPs within the pores of SBA-15 to catalytically reduce 4-NP efficiently [10]. These examples verify Ag NPs as effective catalysts for 4-NP environmental remediation.

Unfortunately, Ag NPs tend to self-aggregate together because of the high surface free energy, leading to obvious decrease of their surface areas [11]. To improve the catalytic performance and stability, it is feasible to incorporate Ag NPs with another metal such as Pt [12]. To this regard, bimetallic noble metals with alloy- [13], core-shell [14] and hetero- [15] nanostructures have drawn significant interest, mainly due to the improved catalytic performances in contrast with monometallic counterparts [16]. Among them, core-shell structures are rich in defects and rough surfaces, which would maximize the synergistic effects of the bimetals and eventually contribute to the catalytic characters [17,18]. For example, reduced graphene oxide (RGO) supported hollow Ag@Pt core-shell nanospheres (hAg@Pt-RGO) showed the improved electrocatalytic activity and durability toward ethylene glycol oxidation [19].

Many methods have been developed to synthesize bimetallic core-shell architectures, including seeding growth [20], electroless plating [21], and surface reduction [22]. Jiang's group developed a sequential deposition-reduction method to synthesize Au@Ag core-shell particles on metal-organic frameworks [23]. Chen et al. fabricated Ag/Pt core-shell crystals by depositing Pt over Ag colloidal seeds via a seed-growth method [24]. Unfortunately, the aforementioned synthetic procedures are usually time-consuming and complicated [25].

Poly(ethyleneimine) (PEI, Fig. S1, Supporting Information, SI) has wide application in industry as water soluble polymer [26], owing to its unique surface property and strong chelating ability [27]. For example, Cu NPs were prepared with PEI as a protecting agent [28]. In another case, PEI was adopted to attach Au seeds onto magnetite particles, effectively preventing them from larger aggregates [29].

In the present work, a facile PEI-assisted one-pot approach was developed for constructing highly branched Pt@Ag core-shell nanoparticles (Pt@Ag NPs) in the alkaline solution at room temperature. Their catalytic performance was evaluated by utilizing the catalytic reduction of 4-NP as a model system.

2. Experimental

2.1. Synthesis of highly branched Pt@Ag NPs

For typical fabrication of highly branched Pt@Ag NPs, 1.50 mL of PEI (0.5%) was firstly dissolved into water, followed by sequentially adding 1.00 mL of $AgNO_3$ solution (2 mM) and 0.52 mL of H_2PtCl_6 solution (2 mM) under vigorous stirring at 25 °C. Afterwards, the pH was adjusted to 10.0 with a freshly-prepared NaOH solution (10 mM). Next, 0.10 mL of a hydrazine hydrate solution (0.1 M) was dropwise injected into the above mixture, causing instant color change from yellow to black. After reacting for 30 min at room temperature, the final product was collected by centrifugation at 6000 rpm, and completely washed with water and ethanol, finally drying under vacuum at 60 °C for 24 h.

For comparison, monometallic Ag NPs were prepared by only using $AgNO_3$ as the precursor, while the other experimental conditions were kept the same.

2.2. Catalytic reduction of 4-NP

The catalytic properties of the highly branched Pt@Ag NPs were investigated by UV–visible (vis) spectroscopy *via* the conversion of 4-NP to 4-AP as a benchmarked model, using $NaBH_4$ as a reductant. Typically, 2.70 mL of an aqueous 4-NP solution (0.10 mM) was mixed with 0.30 mL of a freshly-prepared $NaBH_4$ solution (0.10 mM). It is observed that the mixture turns from light yellow to bright yellow. Subsequently, after adding 0.05 mL of the obtained Pt@Ag NPs suspension (1.0 mg mL^{-1}), the reaction was immediately launched and the solution color vanished quickly. The reduction progress was simultaneously monitored by UV–vis spectroscopy. The absorption peak intensities at 400 nm decrease as a function of the reaction time, which corresponds well to the reduction of 4-NP [30]. For comparison, Ag NPs and commercial Pt black were also used as the contrary catalysts under the identical conditions.

The recyclability of 4-NP was examined based on the previous work [31]. In the recycling test, 0.50 mL of a 4-NP solution (7 mM) was sequentially mixed with 1.00 mL of water and 1.00 mL of a freshly-prepared $NaBH_4$ solution, followed by injecting 0.05 mL of the highly branched Pt@Ag NPs suspension (1 mg mL^{-1}). After the first cycle, another 0.05 mL of the 4-NP solution was added to the system again for next cycle.

More detailed information of *Materials* and *Characterization* were offered in SI.

3. Results and discussion

3.1. Characterization

Transmission electron microscopy (TEM) was first employed to investigate the morphology and structure of the typical product. Fig. 1A and C displays the low- and medium-magnification TEM images, which shows a lot of well-defined particles with good dispersion. Moreover, each particle contains a dark center and a gray shell incorporating many highly branch-like structures. It confirms the formation of the core-shell structure. Additionally, the particle size is mainly located in the range of 100–200 nm, with a mean size of 185.47 nm (Fig. 1B).

High-resolution TEM image of the sample exhibits many well-defined lattice fringes. Furthermore, the lattice fringes taken from the marked sections on the shells are very clear, highly ordered and continuous, with a lattice spacing of 0.24 nm (Fig. 1E and F), which well correspond to the (1 1 1) planes of Ag (JCPDS 04-0783) [32]. These observations show the generation of the external Ag shell and the inner Pt core, which are completely consistent with the above TEM analysis. Moreover, the boundaries (Fig. 1E and F) exhibit a wavy-like undulating structure, reflecting the rich defects on the surface and low coordination atom steps [33]. The atomic steps and structural defects show abundant active sites available for catalysis [34].

The selected area electron diffraction (SAED, Fig. 1D) pattern exhibits the diffraction rings from inner to outside, which are originated from the (1 1 1), (2 0 0), (2 2 0) and (3 1 1) planes of the *fcc* structure, respectively, reflecting the polycrystalline character of the synthesized Pt@Ag NPs.

High-angle annular dark-field scanning transmission electron microscopy-energy dispersive spectroscopy (HAADF-STEM-EDS) experiments were used to check the compositions and their distribution (Fig. 2A–C) [35]. Notably, Pt atoms mainly emerge in the inner section, while Ag atoms show up evenly around the boundaries. The line scanning profiles (Fig. 2D) further certify the formation of the core-shell frameworks. Additionally, the EDS analysis validates that the atomic ratio of Ag against Pt is 48.80:51.20 (Fig. 2E), which is consistent with the ICP-MS analysis (49.67: 50.33).

X-ray diffraction (XRD) analysis was employed to investigate the chemical composition and crystalline structure, using standard XRD patterns of pure Ag and Pt as the references. Fig. 3 displays

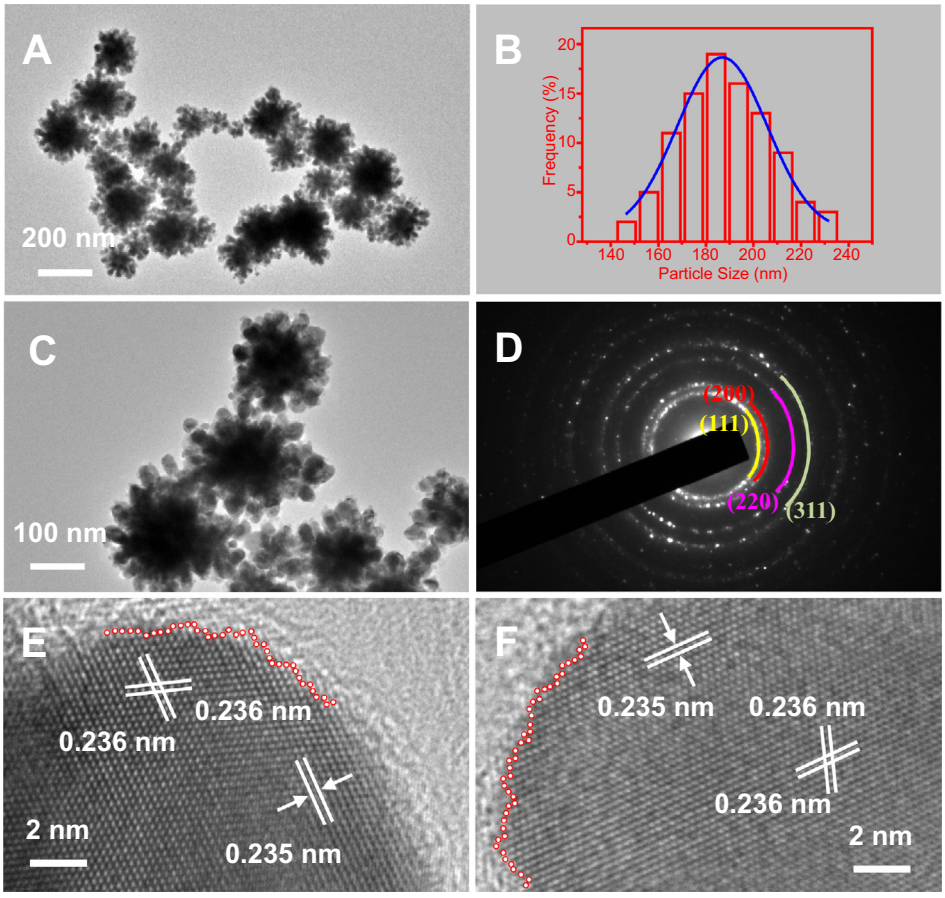

Fig. 1. Low- (A), medium- (C), and high-resolution (E, F) TEM images of highly branched Pt@Ag NPs. (B) and (D) show the particle-size distribution and SAED pattern, respectively.

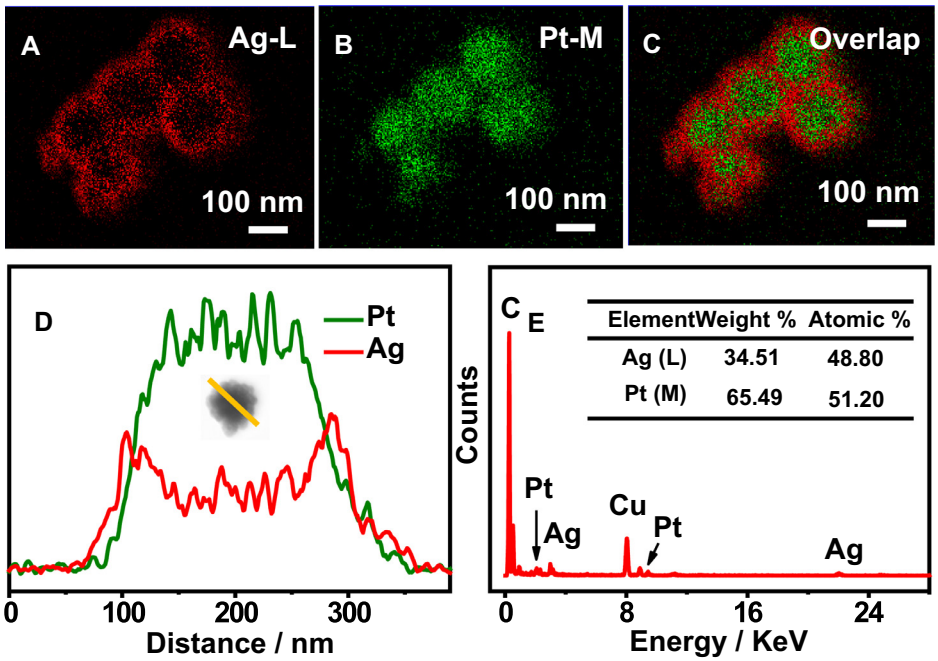

Fig. 2. HAADF-STEM-EDS mappings (A–C) of highly branched Pt@Ag NPs. (D) Cross-sectional compositional line scanning profiles and (E) EDS spectrum. Inset in (E) shows the elemental atomic ratios.

four strong diffraction peaks at 38.18°, 44.70°, 66.90°, and 80.85°, which are attributed to the (1 1 1), (2 0 0), (2 2 0), and (3 1 1) planes of the face centered cubic (*fcc*) bulk Ag [36]. Meanwhile, the weak shoulder peak located at near each main peak certifies the appearance of the internal Pt core, further demonstrating the formation of the core-shell Pt@Ag architectures [8].

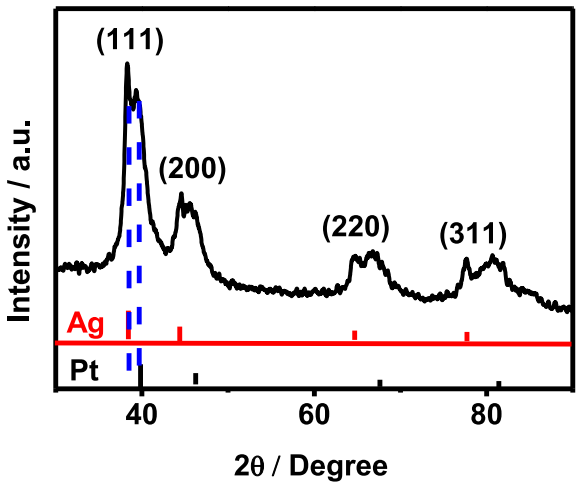

Fig. 3. XRD spectrum of highly branched Pt@Ag NPs. Standard XRD patterns of bulk Pt (JCPDS-04-0802) and Ag (JCPDS-04-0783) were provided for comparison.

The chemical valence and composition are further verifies by X-ray photoelectron spectroscopy (XPS) [37]. As seen from the high-resolution Ag 3d XPS spectrum, there are two peaks located at 373.37 eV (Ag $3d_{3/2}$) and 367.35 eV (Ag $3d_{6/2}$), belonging to metallic Ag^0 (Fig. 4A). It reveals that the Ag precursor is completely reduced to metallic Ag [38].

Meanwhile, the Pt XPS segment is mainly divided into two pairs of peaks (Fig. 4B). Specifically, the stronger couple at 75.7 and 72.4 eV is ascribed to metallic Pt^0, while the weaker one at 77.1 and 73.4 eV is attributed to $PtO/Pt(OH)_2$ [39]. Based on the peak areas, the atomic ratio of Pt^0/Pt^{2+} is estimated to be 3.95:1.30, and hence metallic Pt^0 is the predominant, indicating the complete reduction of $PtCl_6^{2-}$ in this synthesis [40]. By combining the calculation of the XPS data (Fig. 4), the atomic ratio of Ag against Pt is estimated to be 54.04:45.96 on the surface, slightly higher than that obtained from the EDS or ICP analysis, which might be ascribed to the core-shell structures.

3.2. Formation mechanism of highly branched Pt@Ag NPs

Herein, series of controlled experiments were performed to depict the formation mechanism of the highly branched Pt@Ag NPs. As Fig. S2A (SI) illuminates, insufficient PEI (0.2%) induces the formation of much aggregated particles with broad size-distribution, very unlike the typical Pt@Ag NPs at 0.5% PEI (Fig. 1). Alternatively, sufficient PEI yields small grains without any specific morphology (e.g. 1.0% PEI, Fig. S2B, SI). These phenomena demonstrate that PEI acts as a structure director to efficiently tune the size and shape during the synthesis. It is mainly attributed to the strong chelating ability and electrostatic interactions of PEI with the metal salts [41].

Specifically, PEI has great impacts on the reduction potentials (i.e. Ag^+ and $PtCl_6^{2-}$), as depicted by linear sweep voltammetry (LSV) curves (Fig. S3, SI). The reduction potentials of Ag^+/Ag (Fig. S3A, SI) and $PtCl_6^{2-}/Pt$ (Fig. S3B, SI) are 0.541 V and 0.617 V in the absence of PEI, respectively, while they have obvious positive shifts after the addition of PEI. What's more, the reduction potential of $PtCl_6^{2-}/Pt$ has the larger shift (0.888 V) alternative to that of Ag^+/Ag (0.592 V) under the identical conditions (Fig. S3C, SI). It means that the PEI-$PtCl_6^{2-}$ complexes preferentially reduce to form initial Pt cores in the system.

In order to deeply uncover the growth mechanism of Pt@Ag NPs, the intermediates at different reaction time were collected for investigation. Fig. S4 (SI) depicts the TEM images. At the reaction time of 5 min (Fig. S4A (SI)), many small irregular particles emerge. The heterogeneous pompon-like structures gradually appear by extending the time to 15 min (Fig. S4B (SI)). By further prolonging the time (i.e. 30 min), the well-defined core-shell particles with highly branch-like structures are generated (Fig. 1).

Taken together, Fig. 5 describes the formation mechanism of highly branched Ag@Pt NPs. Firstly, the two precursors initially complex with PEI in the aqueous system. After adding the hydrazine hydrate, the PEI-$PtCl_6^{2-}$ complexes are preferentially reduced to Pt atoms, which are stabilized by the adjacent PEI molecules. Then, Pt atoms continuously transform to Pt nuclei to minimize the overall surface free energy, thereby forming spherical Pt particles [42]. At the same time, PEI molecules would selectively adsorb onto the (1 1 1) planes of Pt to guide the subsequent deposition of the metallic crystals. Under the guidance of PEI for the oriented growth, the reduction of the Ag precursor occurs and highly-branched Ag shell appear around the Pt nuclei after complete consumption of the Pt precursor, eventually forming highly branched Pt@Ag NPs.

3.3. Catalytic performance of highly branched Pt@Ag NPs

Generally, it is common to examine the catalytic performances of photocatalysts *via* the reduction of 4-NP to 4-AP as a model system, with $NaBH_4$ behaved as a reducing agent [43]. More impressively, the strong absorption peak at 316 nm shifts to 400 nm after the addition of $NaBH_4$ in the aqueous system, due to the formation of 4-nitrophenolate anions (Fig. 6A) [30]. Fig. 7 exhibits the time-dependent UV–vis absorption spectra with the as-prepared highly branched Pt@Ag NPs by using home-made Ag NPs and commercial Pt black as the contrasts. As Fig. 7A displays, the peak

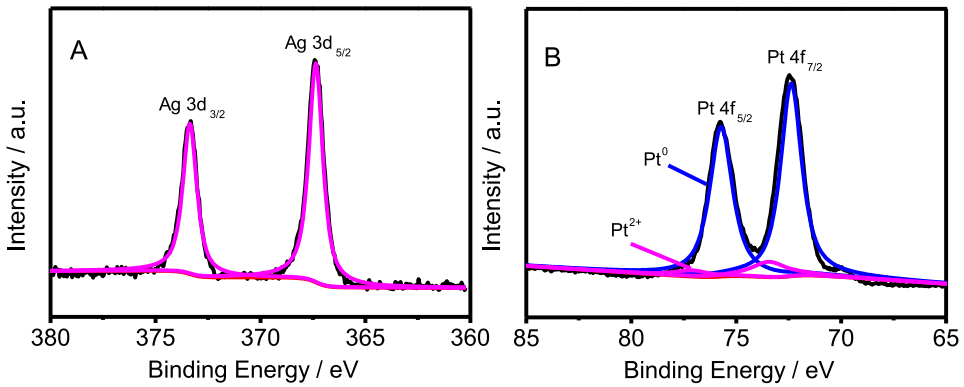

Fig. 4. High-resolution (A) Ag 3d and (B) Pt 4f XPS spectra of the Pt@Ag NPs.

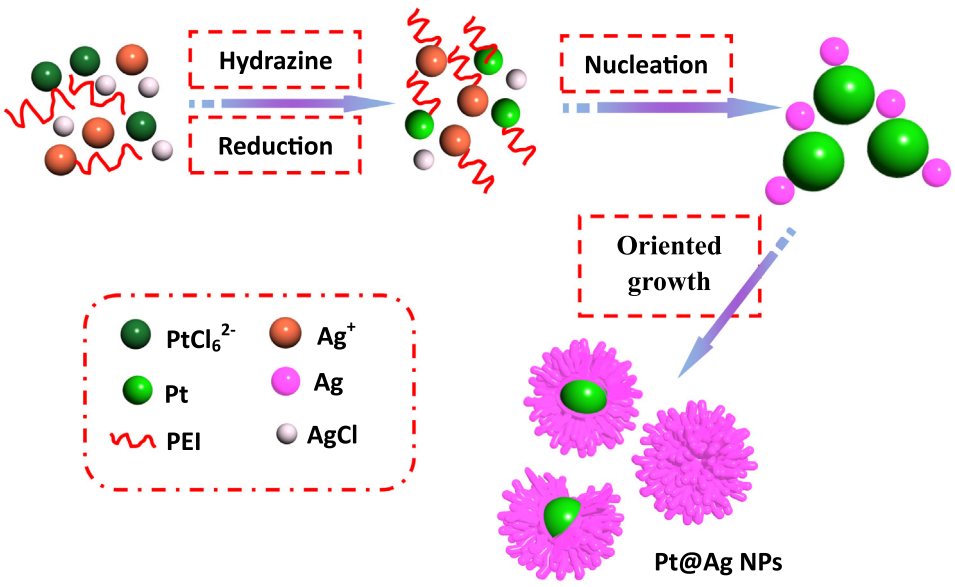

Fig. 5. Schematic illustration of the formation mechanism of the Pt@Ag NPs.

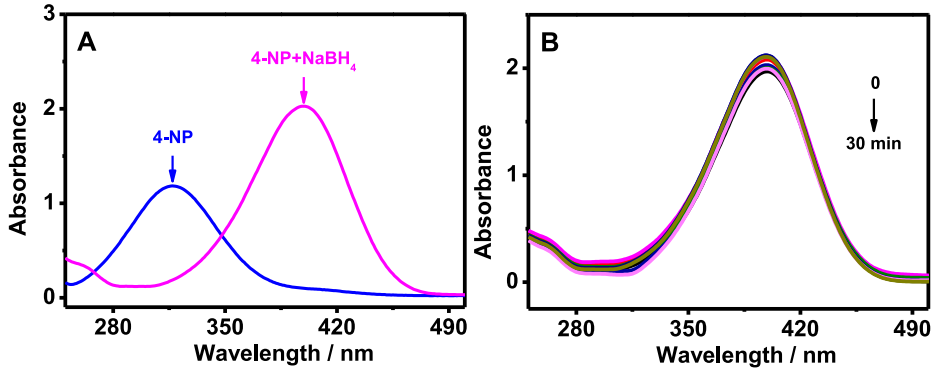

Fig. 6. UV–vis absorption spectra (A) of 4-NP before and after the addition of $NaBH_4$. The time-dependent UV–vis absorption spectra without any catalyst (B).

intensity of 4-NP at 400 nm significantly decreases in the presence of the Pt@Ag NPs, along with the emergence of a new peak at 300 nm originated from 4-AP [4], reflecting the efficient transformation of 4-NP to 4-AP without any other by-product [44]. This observation has much difference from that without any catalyst, where the peak almost remains constant even by further extending the reaction time (Fig. 6B), due to the failure of the reaction without any catalyst.

Moreover, the reduction rate is dramatically facilitated by the Pt@Ag NPs catalyst, which is finished within 8 min. This value is much shorter than those of home-made Ag NPs (Fig. 7B, 20 min) and commercial Pt black (Fig. 7C, 35 min) under the similar conditions, reflecting the superior catalytic property of Pt@Ag NPs. Besides, the reaction time is smaller than those of Ni NPs (60 min) [45] and Au NPs-polyaniline (PANI) composite nanosphere (AuNPs@PANI, 20 min) [46]. The catalytic reduction mechanism of 4-NP on Pt@Ag NPs is described in Fig. 8.

Furthermore, the pseudo-first-order kinetics is usually adopted to evaluate the rate constant for the catalytic reaction, because the $NaBH_4$ concentration is much higher than that of 4-NP in the aqueous system [46]. The first-order rate constant (k) of 4-NP was calculated by the following equation: $-kt = \ln(C_t/C_0) = \ln(A_t/A_0)$, where A_t and A_0 represent the absorbance at certain time and initial stage [30], respectively.

For direct comparison of the catalytic performances of the investigated catalysts, linear plots were obtained of $-\ln(A_t/A_0)$ versus (*vs.*) the reaction time. Clearly, the k is found to be 0.355 min^{-1} for Pt@Ag NPs (Fig. 7D), which is much greater than those of the contrary Ag NPs (0.116 min^{-1}) and Pt black (0.047 min^{-1}) under the same conditions, revealing significant enhancement in the catalytic activity of Pt@Ag NPs relative to those of the referenced catalysts. Additionally, this value is also much larger than those of Ag nanoshell-coated cationic polystyrene beads (0.31 min^{-1}) [47], and yolk-shell Au@C (4.8×10^{-4} s^{-1}) [48].

Besides, turnover frequency (TOF) is another important parameter to assess the catalytic efficiency of a catalyst [49]. The TOF is about 0.088 mol g^{-1} min^{-1} for Pt@Ag NPs, which is higher than those of Ag NPs (0.035 mol g^{-1} min^{-1}) and Pt black (0.02 mol g^{-1} - min^{-1}). The higher k value and larger TOF demonstrate Pt@Ag NPs as an efficient catalyst for reduction of 4-NP.

It is significant for a catalyst to explore its stability and recyclability [50]. The obtained Pt@Ag NPs catalyst was reused in the recycling test under the same operation conditions (Fig. 9). The catalyst was recycled and reused for at least five cycles in the test. The conversion efficiency almost remains constant, outperforming those of AuPd NPs and Pt-Ni/RGO nanocatalyst [8,30]. Moreover, the morphology of the catalyst was almost unchanged even after five cycles (Fig. S5, SI). These phenomena strongly prove the good sta-

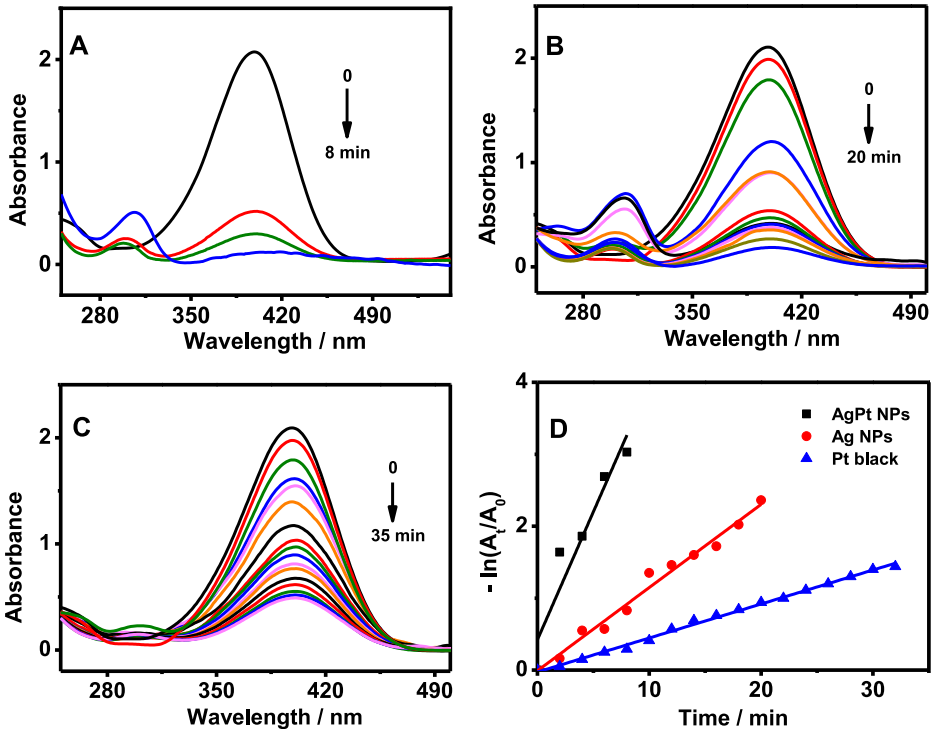

Fig. 7. Time-dependent UV-vis spectral changes of 4-NP reduction catalyzed by the Pt@Ag NPs (A), Ag NPs (B), and Pt black (C). The plots of $-\ln(A_t/A_0)$ *vs.* reaction time (D).

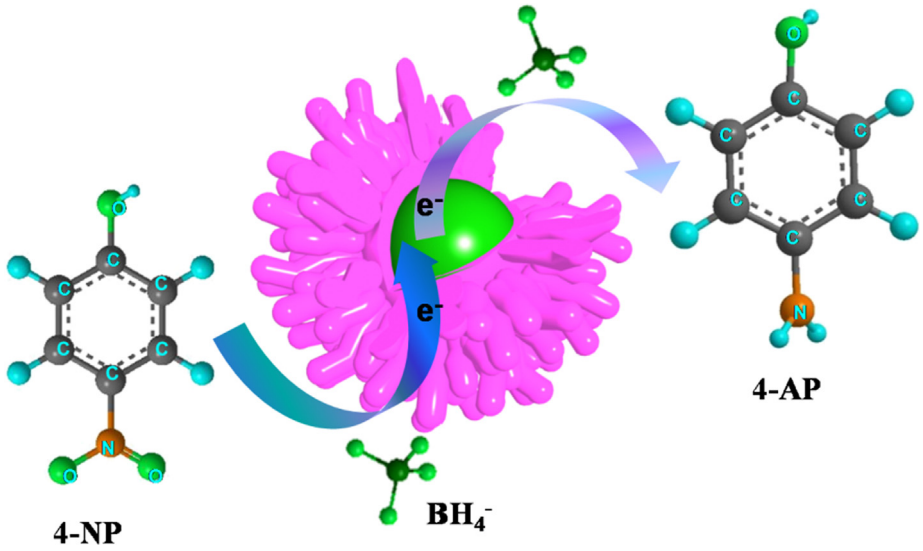

Fig. 8. Schematic illustration of 4-NP catalytic reduction on highly branched Pt@Ag NPs.

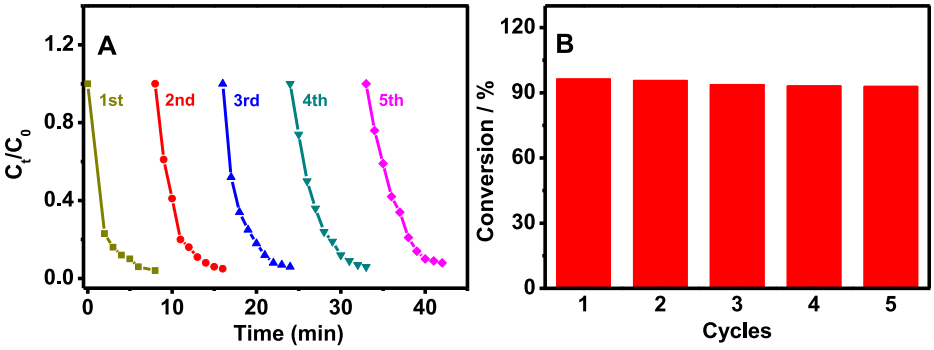

Fig. 9. Plot of C_t/C_0 *vs.* reaction time for 4-NP reduction in five successive cycles (A). The reusability of the Pt@Ag NPs.

bility and acceptable recyclability of the as-prepared catalyst in this research.

The superior catalytic characters of the Pt@Ag NPs catalyst are mainly attributed to the following three aspects: (1) Pt and Ag play the synergistic roles in the catalytic reaction. (2) PEI acts as the structure director that can efficiently prevent Pt@Ag NPs from large aggregates, ultimately modulating their size and shape. (3) The specific core-shell structures provide enriched defects and rough surfaces easily available for 4-NP reduction.

4. Conclusions

In summary, we have developed a simple one-pot wet-chemical strategy for synthesizing highly branched Pt@Ag NPs in the alkaline system, where PEI behaved as the structure-directing agent. In contrast with the contrary catalysts, the fabricated Pt@Ag NPs exhibited dramatically improved catalytic activity, superior stability and recyclability for reducing 4-NP under the similar circumstance. The as-synthesized catalyst has potential applications in catalysis and the developed method can be extended for preparing novel bimetallic nanocatalysts.

Acknowledgments

This work was financially supported by the National Natural Science Foundation of China (No. 21475118) and Zhejiang Province Basic Public Welfare Research Project (LGG18E010001).

Appendix A. Supplementary material

Supplementary data to this article can be found online at https://doi.org/10.1016/j.jcis.2018.11.109.

References

[1] J. Liu, H. Bai, Y. Wang, Z. Liu, X. Zhang, D.D. Sun, Self-assembling TiO_2 nanorods on large graphene oxide sheets at a two-phase interface and their anti-recombination in photocatalytic applications, Adv. Funct. Mater. 20 (2010) 4175–4181.
[2] N. Daneshvar, M.A. Behnajady, Y. Zorriyeh Asghar, Photooxidative degradation of 4-nitrophenol (4-NP) in UV/H_2O_2 process: influence of operational parameters and reaction mechanism, J. Hazard. Mater. 139 (2007) 275–279.
[3] D. Chen, A.K. Ray, Photodegradation kinetics of 4-nitrophenol in TiO_2 suspension, Water Res. 32 (1998) 3223–3234.
[4] K. Kuroda, T. Ishida, M. Haruta, Reduction of 4-nitrophenol to 4-aminophenol over Au nanoparticles deposited on PMMA, J. Mol. Catal. A: Chem. 298 (2009) 7–11.
[5] S. Jobling, J.P. Sumpter, Detergent components in sewage effluent are weakly oestrogenic to fish: an in vitro study using rainbow trout (*Oncorhynchus mykiss*) hepatocytes, Aquat. Toxicol. 27 (1993) 361–372.
[6] E. Caro, R.M. Marcé, P.A.G. Cormack, D.C. Sherrington, F. Borrull, On-line solid-phase extraction with molecularly imprinted polymers to selectively extract substituted 4-chlorophenols and 4-nitrophenol from water, J. Chromatogr. A 995 (2003) 233–238.
[7] H. Ataee Esfahani, L. Wang, Y. Nemoto, Y. Yamauchi, Synthesis of bimetallic Au@Pt nanoparticles with Au core and nanostructured Pt shell toward highly active electrocatalysts, Chem. Mater. 22 (2010) 6310–6318.
[8] F. Zhao, W. Kong, Z. Hu, J. Liu, Y. Zhao, B. Zhang, Tuning the performance of Pt-Ni alloy/reduced graphene oxide catalysts for 4-nitrophenol reduction, RSC Adv. 6 (2016) 79028–79036.
[9] P. Liu, M. Zhao, Silver nanoparticle supported on halloysite nanotubes catalyzed reduction of 4-nitrophenol (4-NP), Appl. Surf. Sci. 255 (2009) 3989–3993.
[10] B. Naik, S. Hazra, V.S. Prasad, N.N. Ghosh, Synthesis of Ag nanoparticles within the pores of SBA-15: an efficient catalyst for reduction of 4-nitrophenol, Catal. Commun. 12 (2011) 1104–1108.
[11] J. Zhang, M. Zhang, K. Tang, F. Verpoort, T. Sun, Polymer-based stimuli-responsive recyclable catalytic systems for organic synthesis, Small 10 (2014) 32–46.
[12] M.k. Min, J. Cho, K. Cho, H. Kim, Particle size and alloying effects of Pt-based alloy catalysts for fuel cell applications, Electrochim. Acta 45 (2000) 4211–4217.
[13] S. Zhang, Y. Shao, H.g. Liao, J. Liu, I.A. Aksay, G. Yin, Y. Lin, Graphene decorated with PtAu alloy nanoparticles: facile synthesis and promising application for formic acid oxidation, Chem. Mater. 23 (2011) 1079–1081.
[14] L. Wang, Y. Yamauchi, Autoprogrammed synthesis of triple-layered Au@Pd@Pt core-shell nanoparticles consisting of a Au@Pd bimetallic core and nanoporous Pt shell, J. Am. Chem. Soc. 132 (2010) 13636–13638.
[15] Z. Peng, H. Yang, Synthesis and oxygen reduction electrocatalytic property of Pt-on-Pd bimetallic heteronanostructures, J. Am. Chem. Soc. 131 (2009) 7542–7543.
[16] D. Wang, Y. Li, Bimetallic nanocrystals: bimetallic nanocrystals: Liquid-phase synthesis and catalytic applications, Adv. Mater. 23 (2011). 1036 1036.
[17] S.H. Joo, J.Y. Park, C.K. Tsung, Y. Yamada, P. Yang, G.A. Somorjai, Thermally stable Pt/mesoporous silica core-shell nanocatalysts for high-temperature reactions, Nat. Mater. 8 (2008) 126.
[18] D.N. Li, F.Q. Shao, J.J. Feng, J. Wei, Q.L. Zhang, A.J. Wang, Uniform Pt@Pd nanocrystals supported on N-doped reduced graphene oxide as catalysts for effective reduction of highly toxic chromium(VI), Mater. Chem. Phys. 205 (2018) 64–71.
[19] J.N. Zheng, J.J. Lv, S.S. Li, M.W. Xue, A.J. Wang, J.J. Feng, One-pot synthesis of reduced graphene oxide supported hollow Ag@Pt core-shell nanospheres with enhanced electrocatalytic activity for ethylene glycol oxidation, J. Mater. Chem. A 2 (2014) 3445–3451.
[20] J.M. Yan, X.B. Zhang, T. Akita, M. Haruta, Q. Xu, One-step seeding growth of magnetically recyclable Au@Co core-shell nanoparticles: highly efficient catalyst for hydrolytic dehydrogenation of ammonia borane, J. Am. Chem. Soc. 132 (2010) 5326–5327.
[21] G.Z. Zou, M.S. Cao, L. Zhang, J. Gang Li, H. Xu, Y.J. Chen, A nanoscale core-shell of β-SiCP-Ni prepared by electroless plating at lower temperature, Surf. Coat. Technol. 201 (2006) 108–112.
[22] T. Endo, K. Kerman, N. Nagatani, H.M. Hiepa, D.K. Kim, Y. Yonezawa, K. Nakano, E. Tamiya, Multiple label-free detection of antigen-antibody reaction using localized surface plasmon resonance-based core-shell structured nanoparticle layer nanochip, Anal. Chem. 78 (2006) 6465–6475.
[23] H.L. Jiang, T. Akita, T. Ishida, M. Haruta, Q. Xu, Synergistic catalysis of Au@Ag core-shell nanoparticles stabilized on metal-organic framework, J. Am. Chem. Soc. 133 (2011) 1304–1306.
[24] L. Chen, W. Zhao, Y. Jiao, X. He, J. Wang, Y. Zhang, Characterization of Ag/Pt core-shell nanoparticles by UV-vis absorption, resonance light-scattering techniques, Spectrochim. Acta, Part A 68 (2007) 484–490.
[25] F.R. Fan, D.Y. Liu, Y.F. Wu, S. Duan, Z.X. Xie, Z.Y. Jiang, Z.Q. Tian, Epitaxial growth of heterogeneous metal nanocrystals: from gold nano-octahedra to palladium and silver nanocubes, J. Am. Chem. Soc. 130 (2008) 6949–6951.
[26] L. Yan, W.T.S. Huck, X.M. Zhao, G.M. Whitesides, Patterning thin films of poly (ethylene imine) on a reactive SAM using microcontact printing, Langmuir 15 (1999) 1208–1214.
[27] F. Qu, Q. Li, J. You, Fluorescent silver nanoclusters capped by polyethyleneimine with different molecular weights: universal synthesis and application as a temperature sensor, J. Lumin. 177 (2016) 133–138.
[28] P. Pulkkinen, J. Shan, K. Leppänen, A. Känsäkoski, A. Laiho, M. Järn, H. Tenhu, Poly(ethylene imine) and tetraethylenepentamine as protecting agents for metallic copper nanoparticles, ACS Appl. Mater. Interfaces 1 (2009) 519–525.
[29] I.Y. Goon, L.M.H. Lai, M. Lim, P. Munroe, J.J. Gooding, R. Amal, Fabrication and dispersion of gold-shell-protected magnetite nanoparticles: systematic control using polyethyleneimine, Chem. Mater. 21 (2009) 673–681.
[30] X. Chen, Z. Cai, X. Chen, M. Oyama, AuPd bimetallic nanoparticles decorated on graphene nanosheets: their green synthesis, growth mechanism and high catalytic ability in 4-nitrophenol reduction, J. Mater. Chem. A 2 (2014) 5668–5674.
[31] P. Song, L.L. He, A.J. Wang, L.P. Mei, S.X. Zhong, J.R. Chen, J.J. Feng, Surfactant-free synthesis of reduced graphene oxide supported porous PtAu alloyed nanoflowers with improved catalytic activity, J. Mater. Chem. A 3 (2015) 5321–5327.
[32] M.R. Hajmohammadi, H. Maleki, G. Lorenzini, S.S. Nourazar, Effects of Cu and Ag nano-particles on flow and heat transfer from permeable surfaces, Adv. Powder Technol. 26 (2015) 193–199.
[33] L.Y. Jiang, X.X. Lin, A.J. Wang, J. Yuan, J.J. Feng, X.S. Li, Facile solvothermal synthesis of monodisperse $Pt_{2.6}Co_1$ nanoflowers with enhanced electrocatalytic activity towards oxygen reduction and hydrogen evolution reactions, Electrochim. Acta 225 (2017) 525–532.
[34] T. Fujita, P. Guan, K. McKenna, X. Lang, A. Hirata, L. Zhang, T. Tokunaga, S. Arai, Y. Yamamoto, N. Tanaka, Y. Ishikawa, N. Asao, Y. Yamamoto, J. Erlebacher, M. Chen, Atomic origins of the high catalytic activity of nanoporous gold, Nat. Mater. 11 (2012) 775.
[35] D.B. Huang, Q. Yuan, P.L. He, K. Wang, X. Wang, A facile and general strategy for the synthesis of porous flowerlike Pt-based nanocrystals as effective electrocatalysts for alcohol oxidation, Nanoscale 8 (2016) 14705–14710.
[36] Y.W. Lee, M. Kim, Z.H. Kim, S.W. Han, One-step synthesis of Au@Pd core-shell nanooctahedron, J. Am. Chem. Soc. 131 (2009) 17036–17037.
[37] L.M. Rivera Gavidia, G. García, D. Anaya, A. Querejeta, F. Alcaide, E. Pastor, Carbon-supported Pt-free catalysts with high specificity and activity toward the oxygen reduction reaction in acidic medium, Appl. Catal. B Environ. 184 (2016) 12–19.
[38] Y. Yang, W. Wang, Y. Liu, F. Wang, Z. Zhang, Z. Lei, Carbon supported heterostructured Pd-Ag nanoparticle: highly active electrocatalyst for ethylene glycol oxidation, Int. J. Hydrogen Energy 40 (2015) 2225–2230.

[39] L.L. He, J.N. Zheng, P. Song, S.X. Zhong, A.J. Wang, Z. Chen, J.J. Feng, Facile synthesis of platinum-gold alloyed string-bead nanochain networks with the assistance of allantoin and their enhanced electrocatalytic performance for oxygen reduction and methanol oxidation reactions, J. Power Sources 276 (2015) 357–364.
[40] L.X. Chen, L. Liu, J.J. Feng, Z.G. Wang, A.J. Wang, Oligonucleotide-assisted successive coreduction synthesis of dendritic platinum-gold core-shell alloy nanocrystals with improved electrocatalytic performance for methanol oxidation, J. Power Sources 302 (2016) 140–145.
[41] Y.C. Shi, S.S. Chen, J.J. Feng, X.X. Lin, W. Wang, A.J. Wang, Dicationic ionic liquid mediated fabrication of Au@Pt nanoparticles supported on reduced graphene oxide with highly catalytic activity for oxygen reduction and hydrogen evolution, Appl. Surf. Sci. 441 (2018) 438–447.
[42] Y.C. Shi, J.J. Feng, S.S. Chen, G.M. Tu, J.R. Chen, A.J. Wang, Simple synthesis of hierarchical AuPt alloy nanochains for construction of highly sensitive hydrazine and nitrite sensors, Mater. Sci. Eng. C 75 (2017) 1317–1325.
[43] X. Huang, Y. Li, H. Zhou, X. Zhong, X. Duan, Y. Huang, Simplifying the creation of dumbbell-like Cu-Ag nanostructures and their enhanced catalytic activity, Chem. – Eur. J. 18 (2012) 9505–9510.
[44] Y. Imura, K. Tsujimoto, C. Morita, T. Kawai, Preparation and catalytic activity of Pd and bimetallic Pd-Ni nanowires, Langmuir 30 (2014) 5026–5030.
[45] N. Sahiner, H. Ozay, O. Ozay, N. Aktas, New catalytic route: Hydrogels as templates and reactors for in situ Ni nanoparticle synthesis and usage in the reduction of 2- and 4-nitrophenols, Appl. Catal. A 385 (2010) 201–207.
[46] R. Li, Z. Li, Q. Wu, D. Li, J. Shi, Y. Chen, S. Yu, T. Ding, C. Qiao, One-step synthesis of monodisperse AuNPs@PANI composite nanospheres as recyclable catalysts for 4-nitrophenol reduction, J. Nanopart. Res. 18 (2016).
[47] S. Jana, S.K. Ghosh, S. Nath, S. Pande, S. Praharaj, S. Panigrahi, S. Basu, T. Endo, T. Pal, Synthesis of silver nanoshell-coated cationic polystyrene beads: a solid phase catalyst for the reduction of 4-nitrophenol, Appl. Catal., A 313 (2006) 41–48.
[48] B. Guan, X. Wang, Y. Xiao, Y. Liu, Q. Huo, A versatile cooperative template-directed coating method to construct uniform microporous carbon shells for multifunctional core-shell nanocomposites, Nanoscale 5 (2013) 2469–2475.
[49] M. Liang, R. Su, W. Qi, Y. Zhang, R. Huang, Y. Yu, L. Wang, Z. He, Reduction of hexavalent chromium using recyclable Pt/Pd nanoparticles immobilized on procyanidin-grafted eggshell membrane, Ind. Eng. Chem. Res. 53 (2014) 13635–13643.
[50] A. Gangula, R. Podila, R. M, L. Karanam, C. Janardhana, A.M. Rao, Catalytic reduction of 4-nitrophenol using biogenic gold and silver nanoparticles derived from breynia rhamnoides, Langmuir 27 (2011) 15268–15274.